Design and Validation of a Scale-Adaptive Filtering Technique for LRN Turbulence Modeling of Unsteady Flow

W. Gyllenram

H. Nilsson

Division of Fluid Dynamics,
Department of Applied Mechanics,
Chalmers University of Technology,
SE-412 96 Gothenburg, Sweden

An adaptive low-pass filtering procedure for the modeled turbulent length and time scales is derived and applied to Wilcox' original low reynolds number k-ω turbulence model. It is shown that the method is suitable for complex industrial unsteady flows in cases where full large eddy simulations (LESs) are unfeasible. During the simulation, the modeled length and time scales are compared to what can potentially be resolved by the computational grid and time step. If the modeled scales are larger than the resolvable scales, the resolvable scales will replace the modeled scales in the formulation of the eddy viscosity. The filtered k-ω model is implemented in an in-house computational fluid dynamics (CFD) code, and numerical simulations have been made of strongly swirling flow through a sudden expansion. The new model surpasses the original model in predicting unsteady effects and producing accurate time-averaged results. It is shown to be superior to the wall-adpating local eddy-viscosity (WALE) model on the computational grids considered here, since the turbulence may not be sufficiently resolved for an accurate LES. Because of the adaptive formulation, the filtered k-ω model has the potential to be successfully used in any engineering case where an LES is unfeasible and a Reynolds (ensemble) averaged Navier–Stokes simulation is insufficient.
[DOI: 10.1115/1.2911685]

1 Introduction

The standard two-equation eddy viscosity turbulence models are designed to predict the influence of all turbulent scales. In doing this, they have a strong damping influence on any resolved turbulence or unsteady structures in the flow field. This is desireable in steady calculations, in which the influence of any unsteadiness on the mean flow field must, by definition, be modeled. However, when unsteady information about the flow field is necessary, the turbulence model must be able to distinguish between resolvable and nonresolvable scales. In this paper, it will be shown that this ability can be achieved by applying a low-pass filter to the modeled turbulent length and time scales.

There are many interesting strategies for unsteady turbulence modeling. Spalart [1] gave an overview and discussion about the advantages and limitations of many of these. As the Reynolds numbers of most engineering flows are usually very large, large eddy simulation (LES) is very seldom an option for a full scale industrial simulation. On the other hand, traditional statistical turbulence models developed for the Reynolds (ensemble) averaged Navier–Stokes (RANS) equations do not distinguish between unsteadiness and turbulence. This problem partly arises from the fact that most industrial closure models for the RANS equations are tuned for steady flow, in which the model must predict the influence of all turbulent time scales and, subsequently, all turbulent length scales. In a time-resolved computation, there is a potential in resolving large turbulent time scales. In addition, the grid is usually capable of resolving the largest turbulent length scales, at least outside boundary layers. In a numerical simulation of an unsteady internal (wall-bounded) flow, in which the boundary layer is not fully resolved, models that are tuned to steady flow usually behave very well in the near-wall region. Statistical turbulence models are generally quite accurate in their prediction of wall shear stress. However, there is also a conceptual aspect of the aforementioned problem with statistical turbulence models. In general, there is no way to mathematically distinguish unsteadiness from turbulence. Although the uniqueness of a solution to the three-dimensional Navier–Stokes equations has yet to be mathematically proven [2], it is generally accepted to believe that the solution is completely determined by the initial and boundary conditions. If this is the case, there are no such things as randomness or independent events in the flow. The lack of coherence we observe in a turbulent flow field only gives us a hint of our limited perception. Hence, the concept of ensemble averaging is questionable in unsteady computational fluid dynamics (CFD), simply because one expects to get the same solution repeatedly if one uses the same boundary conditions and the same computer. The ensemble average of an infinite number of direct numerical simulations would thus still be an unsteady and turbulent flow field. The filtering approach of LES is physically more appealing, compared to the concept of ensemble averaging. The limitations of LES are related to a large extent to the simple turbulence models that are used. These models are calibrated to give accurate results if most energy-containing eddies are resolved everywhere, which means that the computational grid has to be extremely fine near walls. Usually, they do not provide any information about how turbulence is convected through the domain. This information is assumed to be carried by the resolved flow field.

There is obviously a need for a turbulence model that can distinguish between what can be resolved and what is not, at the same time as it produces an accurate estimate of the wall shear stress. One method to accomplish this is to introduce a filtering procedure that limits the influence of the statistical turbulence model on the unsteady mean flow field. This is sometimes called very large eddy simulation (VLES) and may be viewed as a combination of the LES and RANS approaches to turbulence modeling. Other common acronyms for the combination of LES and

Contributed by the Fluids Engineering Division of ASME for publication in the JOURNAL OF FLUIDS ENGINEERING. Manuscript received June 11, 2007; final manuscript received; January 11, 2008 published online April 29, 2008. Assoc. Editor: Paul Durbin.

 Copyright © 2008 by ASME

Downloaded 30 Apr 2008 to 129.16.64.122. Redistribution subject to ASME license or copyright; see http://www.asme.org/terms/Terms_Use.cfm

RANS methods are detached eddy simulation (DES), limited numerical scales (LNSs), extra large eddy simulation (XLES), flow simulation methodology (FSM), or simply hybrid LES-RANS. In a full LES, the Navier–Stokes equations are filtered in space in order to avoid the need of computing the smallest turbulent scales. The equations are usually averaged (filtered) over the control volumes of the grid, and the unresolved scales are regarded as subgrid turbulence. In contrast to LES, where the mean length scales of all unresolved turbulence are assumed proportional to the local grid spacing, VLES is usually based on statistical turbulence models where the turbulent length scale is calculated and will depend on the flow field. Consequently, the filtering procedure can be formulated in a more dynamic and general way compared to the static spatial filtering of a LES. It can be activated locally in the space-time domain depending on the ratio between an estimation of the resolved turbulent length scales and the magnitude of the modeled turbulent length scales. There are many ways of formulating this dynamical filter. Speziale [3,4] and Fasel et al. [5] arbitrarily defined an exponential filter function, $f(\Delta, L_t) = (1 - \exp(\beta\Delta / L_t))^n$, that depends on a predefined length scale, Δ (presumably proportional to the local grid spacing), and a modeled turbulent length scale, L_t, where subscript t denotes turbulence. The exponential function will allow a smooth transition between the RANS and LES modes of the simulation. The function is multiplied to the modeled Reynolds stress tensor before solving the averaged momentum equations in order to limit the effect of the turbulence model on the mean flow field in regions where parts of the tensor can be resolved. As noted by Fasel et al. [5], other forms of the filter function that are more universally applicable may be defined. Another approach to filtering is to limit the length scales in the transport equations for turbulent quantities, as done by Spalart et al. [6], Menter et al. [7,8], Kok et al. [9], and Menter and Egerov [10]. Spalart et al. [6] defined a maximum length scale, $\tilde{L} = \min\{L_{\text{wall}}, C_{\text{DES}}\Delta\}$, to be used in the denominator of the destruction term of the Spalart–Allmaras transport equation for eddy viscosity. In this formulation, L_{wall} is the normal distance to the wall and Δ is again proportional to the local grid spacing. C_{DES} is a model coefficient that must be calibrated. When $L_{\text{wall}} < C_{\text{DES}}\Delta$, the simulation will run in RANS mode. Away from walls, the destruction term in the equation for the eddy viscosity will be significantly larger than in the original formulation, and the simulation will be forced to run in a LES mode. This approach is aptly called DES. Menter et al. [8] used a similar filtering procedure for the shear stress transport (SST) turbulence model. However, as the SST model, is a two-equation model from which a modeled turbulent length scale can be obtained, the filter is formulated in a more dynamic way by comparing the modeled scales of the simulation to the predefined length scale, Δ. This approach is taken a step further by Menter et al. [7] and Menter and Egerov [10], where instead the von Karman length scale is computed from the resolved velocity field and replaces the predefined length scale. In the latter case, all information from both the resolved and unresolved turbulent length scales is obtained from either the resolved velocity field or the turbulence model. Another interesting hybrid LES-RANS method was recently proposed by Templeton et al. [11], in which precomputed lookup tables for the RANS eddy viscosity are used to define wall functions for coarse grid LES. The eddy viscosity that is active in the solution of the LES equations in the near-wall region is here taken as the difference between the RANS eddy viscosity and an averaged resolved eddy viscosity. However, because the resolved eddy viscosity must be averaged, the method is not entirely straightforward if the flow lacks homogeneous directions.

The filtering approach in this work may in some sense be considered converse to the filtering approach that is used in LES. Instead of solving the filtered equations to avoid the computation of the small scales, the modeled length and time scales are filtered in order to supress their negative influence on unsteady flow field. This approach was initially developed by Willems [12] and is similar to the approach of Speziale [3,4] and Fasel et al. [5], because the filter is applied directly to the Reynolds stress tensor and the turbulence model is left unchanged. However, in this work, the functional form of the filter is derived from the relation between filtered and nonfiltered turbulent length and time scales. The modeled length and time scales are being compared to what can potentially be resolved by the computational grid and time step. If the modeled scales are larger than the resolvable scales, the resolvable scales will replace the modeled scales in the formulation of the eddy viscosity. To distinguish between large- and small-scale turbulences, the upper limit of the length scales of nonresolved turbulence is made proportional to the local grid spacing or the product of the local velocity magnitude and the time step of the simulation. The latter constraint will only be active for large Courant, Friedrich, and Levy (CFL) numbers. There is no lower limit because the mean nonresolved turbulent length scale may be much smaller than the local grid spacing, especially close to walls. This will allow a much coarser grid resolution than in LES. The filter will allow large-scale unsteady structures in the flow, and the model will still produce a wall shear stress comparable to what is produced by a standard RANS model. In this work, the filtering technique is applied to the Wilcox' [13] k-ω model, and the results are validated with experimental data (Dellenback et al. [14]) and compared to LES.

2 Filtered Navier–Stokes Equations

There are various filtering approaches for unsteady CFD. They all give rise to new unknowns in the Navier–Stokes equations that must be modeled. The main issue in eddy viscosity models is to determine which length and time scales should be used. It is important to realize that the local value of modeled scales is the *local mean value* of all nonresolved turbulent scales, and the distribution and magnitude of the eddy viscosity are the only parameters that separate a LES from an unsteady RANS simulation. The local mean value may be defined either as an ensemble average (RANS) or a local volume average (LES). The governing equations will nevertheless be identical in their form. However, for conceptual reasons (see Sec. 1), the local volume average is preferable. John [2] made a review of several volume-averaging (filtering) techniques of the Navier–Stokes equations, including estimates of the errors that are associated with the new formulation. The volume-averaged Navier–Stokes equations can be expressed as

$$\partial_0 \bar{u}_i + \bar{u}_j \partial_j \bar{u}_i = -\frac{1}{\rho}\partial_i \bar{p} + \nu \partial_j \partial_j \bar{u}_i - \partial_j \mathcal{R}_{ij} \tag{1}$$

where $\bar{u}_j$ is the resolved (volume-averaged) velocity vector and $\bar{p}$ is the resolved pressure. The Reynolds stress tensor, $\mathcal{R} = -\bar{u}_i\bar{u}_j + \overline{u_i u_j}$, can be expanded into

$$\mathcal{R}_{ij} = -\bar{u}_i\bar{u}_j + \overline{\bar{u}_i\bar{u}_j} + \overline{\bar{u}_i u_j'} + \overline{u_i'\bar{u}_j} + \overline{u_i' u_j'} \tag{2}$$

where Reynolds decomposition, $u_i = \bar{u}_i + u_i'$, has been used. Here, u_i is the exact solution and u_i' denotes a fluctuation from the resolved velocity vector. The turbulence model that will replace the Reynolds stress tensor, $\mathcal{R}_{ij}$, in a numerical simulation must predict a nonresolved turbulent length scale, ℓ_t, that is *smaller or equal* to the averaging length scale, or filter width, Δ_f, which is usually chosen to be proportional to the local grid spacing. Zero- and one-equation subgrid models always use a length scale, ℓ_t, that is proportional to the local grid spacing. However, the length scale, ℓ_t, of the unknown, $u_i'(\mathbf{x}, t)$, does not generally correspond to the length scales of the grid. In near-wall regions, $\ell_t \ll \Delta$, unless the local grid spacing is extremely fine, i.e., near the resolution required for a direct numerical simulation (DNS). Obviously, there is a need for a closure model that can predict length scales that are smaller than the grid spacing, if necessary.

Downloaded 30 Apr 2008 to 129.16.64.122. Redistribution subject to ASME license or copyright; see http://www.asme.org/terms/Terms_Use.cfm

3 Turbulence Modeling

The k-ω model of Wilcox [13], with the addition of the realizability constraint derived by Durbin [15], has been used as the basic turbulence model in this work. The main advantage of this model over, e.g., k-ε models, is that it can be integrated all the way to the wall without damping or correction functions. The model is a two-equation eddy viscosity model, and it is coupled to the averaged Navier–Stokes equations by the Boussinesq assumption,

$$-\mathcal{R}_{ij} = 2\nu_t S_{ij} - \tfrac{2}{3}k\delta_{ij} \tag{3}$$

where $S_{ij}=(\partial_j U_i+\partial_i U_j)/2$ and $k=\overline{u_i' u_i'}/2$ is the turbulent kinetic energy. The Boussinesq assumption introduces the concept of a turbulent eddy viscosity, ν_t. It suggests that the influence of turbulence on the mean flow is dominated by a mixing process. The eddy viscosity has the same dimension as the kinematic viscosity of the fluid and is assumed to be proportional to a function of the local turbulent length and time scales, i.e.,

$$\nu_t \sim L_t^2/T_t \tag{4}$$

The turbulent length and time scales are unknown local properties of the turbulent flow and must be modeled. If transport equations for, e.g., the modeled turbulent kinetic energy, k, and dissipation rate, ε, or specific dissipation rate, ω, are solved, a measure of the turbulent length and time scales can be obtained from these variables by dimensional analysis, see Sec. 3.1.

3.1 Consistent Derivation of the Filter Function. The filtering approach of Willems [12] has earlier been successfully employed by Helmrich et al. [16] and Ruprecht et al. [17]. This filter is applied to the turbulence model in order to allow the existence of resolvable turbulent scales in the solution of the flow field. Willems derived the form of the filter function from the two-point correlation tensor and applied it to the k-ε model. In the present paper, the same form of the filter function is derived by simple dimensional analysis. It is also shown that the novel generalization of the approach to other eddy viscosity models than the k-ε model requires that the filter is applied to the turbulent length and time scales and not only to the turbulent kinetic energy, as in Willems' work.

The local turbulent length and time scales may be obtained from a dimensional analysis of k and ω. It follows that

$$L_t \sim k^{1/2}/\omega \tag{5}$$

$$T_t \sim 1/\omega \tag{6}$$

The filter width, Δ_f, is the upper limit of the modeled turbulent length scale. This corresponds exactly to the lower limit of the resolved turbulent length scale and will in this work be a function of time step δt and local cell volume Δ. Hence, the largest length scale that needs to be a part of the eddy viscosity formulation is

$$\ell_t = \min\{L_t, \Delta_f\} \tag{7}$$

where

$$\Delta_f = \alpha \max\{|\mathbf{U}|\delta t, \Delta^{1/3}\} \tag{8}$$

Coefficient $\alpha > 1$ takes into account the need for a limited number of cells to actually resolve a turbulent structure. In the study by Gyllenram and Nilsson [18], a value of $\alpha \geqslant 3$ was necessary to obtain accurate results. The product $|\mathbf{U}|\delta t$, in Eq. (8), is a measure of the shortest distance, over which a fluid particle can be traced in an unsteady computation, for which reason the computational time step may also set a lower limit to the resolved length scale. This temporal constraint is especially important in complex geometries, as discusseed by Batten et al. [19], who also noted that a steady RANS calculation would correspond to an infinite time step, for which $\ell_t = L_t$, always. The upper limit on the modeled length and time scales can also be defined in terms of the filtered (nonresolved) variables, i.e.,

$$\ell_t \sim \hat{k}^{1/2}/\hat{\omega} \tag{9}$$

$$t_t \sim 1/\hat{\omega} \tag{10}$$

The specific dissipation rate, ω, is related to the dissipation rate, ε, by the relation

$$\omega = \frac{\varepsilon}{\beta^* k} \tag{11}$$

where $\beta^* = 0.09$. The filtered specific dissipation rate can be written as

$$\hat{\omega} = \frac{\hat{\varepsilon}}{\beta^* \hat{k}} \tag{12}$$

The dissipation rate, ε, is never resolved in anything cheaper than a DNS, because it takes action at the Kolmogorov scale, the very smallest turbulent length scale. Hence,

$$\hat{\varepsilon} = \varepsilon \tag{13}$$

and it follows from Eqs. (11)–(13), that

$$\hat{\omega} = \frac{\omega k}{\hat{k}} \tag{14}$$

It is straightforward to show that Eqs. (5), (9), and (14) yield an expression for the filtered turbulent kinetic energy according to

$$\hat{k} = g(\ell_t, L_t)k \tag{15}$$

where the equality follows from the assumption that the constants of proportionality in Eqs. (5) and (9) are equal. The filter function, $g(\ell_t, L_t)$, is defined as

$$g \equiv (\ell_t/L_t)^{2/3} \tag{16}$$

in which ℓ_t is computed from Eq. (7) and the modeled turbulent length scale, L_t, is taken as $L_t = \sqrt{k}/(\beta^*\omega)$. In regions where turbulence cannot be resolved, i.e., where $L_t < \Delta_f$ in Eq. (7), the filter function, Eq. (16), is unity and $\hat{k}=k$ in Eq. (15). However, there is no need to compute the filtered turbulent variables explicitly. A filtered eddy viscosity can be constructed directly from the nonresolvable turbulent length and time scales, i.e.,

$$\hat{\nu}_t \sim \ell_t^2/t_t \tag{17}$$

It follows from Eqs. (9), (10), (14), and (15) that

$$\hat{\nu}_t = g^2 \frac{k}{\omega} \tag{18}$$

where the equality must hold in order to recover the original (nonfiltered) eddy viscosity formulation, $\nu_t = k/\omega$, in regions where the filter is inactive. Note that the only modification to the original eddy viscosity formulation is the factor g^2, i.e., the square of the filter function. The filter function can be derived and applied using *any* two-equation turbulence model. It will always obtain the same functional form as in Eq. (16) and it will always end up as squared when used in the formulation of the eddy viscosity.

There will obviously be an explicit grid dependence in the eddy viscosity formulation, Eq. (18), when $\Delta_f < L_t$ in Eq. (7). However, the derivative of g^2 with respect to the filter width,

$$\frac{\partial(g^2)}{\partial \Delta_f} = \frac{4}{3}\left(\frac{\Delta_f}{L_t}\right)^{1/3} \tag{19}$$

will vanish in the fine grid limit, $\Delta_f \to 0$, because

$$\left.\frac{\partial(g^2)}{\partial \Delta_f}\right|_{\Delta_f \to 0} \to 0 \tag{20}$$

This shows that the eddy viscosity asymptotically approaches a constant in the fine grid limit, as long as the model equations for k and ε do not explicitly depend on the local grid spacing them-

Downloaded 30 Apr 2008 to 129.16.64.122. Redistribution subject to ASME license or copyright; see http://www.asme.org/terms/Terms_Use.cfm

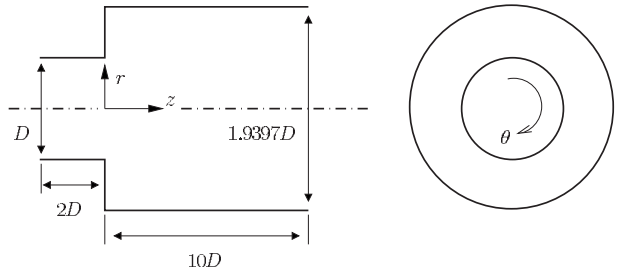

Fig. 1 Geometry of the test case. The inlet swirl is clockwise in the *z* direction.

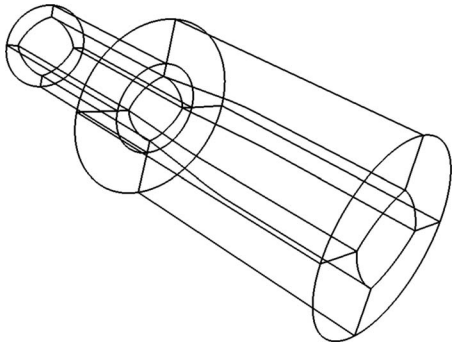

Fig. 2 Block structure. Only 10 out of 15 blocks are shown.

selves. Actually, as the eddy viscosity is limited by the filter, there will also be less production of modeled turbulent kinetic energy, k, and specific dissipation rate, ω. This is natural, because the resolved turbulent kinetic energy and specific dissipation should increase. The importance of the novel approach of applying the filter to the length and time scales of the eddy viscosity formulation instead of only to the turbulent kinetic energy, as in the work of Willems [12], is now obvious. If the filter was applied only to the turbulent kinetic energy, the square of the filter function $g(\ell_t, L_t)$ in Eq. (18) would vanish and the filter would not have the proper behavior in the fine grid limit according to Eq. (20).

3.1.1 Near-Wall Asymptotics. There could be an obvious risk in applying a filter width that is too small in boundary layers because, if $\Delta_f < L_t$ in Eq. (7), the eddy viscosity can be written as

$$\hat{\nu}_t = \beta^* \Delta_f^{4/3} (\beta^* \omega k)^{1/3} \tag{21}$$

This expression does not have the proper asymptotical behavior in the near-wall limit unless the grid is abnormally stretched. In the limit $n \to 0$, where n is the wall-normal coordinate, $\hat{\nu}_t \sim n^{1/3}$, while a proper functional behavior of the eddy viscosity would be $\nu_t \sim n^3$, at least in a time-averaged sense [20]. However, the purpose of the filtering approach is to avoid the need of an extremely fine near-wall resolution and, indeed, the wall boundary condition for the turbulent kinetic energy, $k_{\text{wall}}=0$, is expected to limit the modeled turbulent length scale and thereby inactivate the filter before the wall limit is reached. Nevertheless, too small a filter width (α) may, as shown by Gyllenram and Nilsson [18], cause the filter to be activated all the way to the wall and the results to deteriorate. However, on a computational grid with a wall $y^+ \sim 2$, the modeled turbulent length and time scales obtained from the k-ω model are small enough to inactivate the filter near the wall using $\alpha=3$ in Eq. (8), as will be shown in Sec. 5. In other words, the filter should not be active close to walls. Instead, the underlaying RANS model should take care of the near-wall modeling.

4 Test Case and Computational Setup

A swirling flow through a sudden expansion has been investigated, see Fig. 1. Measurements courtesy of Dellenback et al. [14] have been used to validate the results. The swirl number, defined as

$$S = \frac{\int_0^R V_\theta V_z r^2 dr}{R \int_0^R V_z^2 r dr} \tag{22}$$

is approximately 0.6, based on the inlet radius, $R=D/2$. V_θ and V_z denote the time-averaged tangential and axial velocities, respectively. The Reynolds number, based on the inlet diameter, D, and bulk velocity, U_b, is 30,000. The case has earlier been studied numerically by Schlüter et al. [21] and Gyllenram et al. [22]

4.1 Code. The CALC-PMB [23] CFD software was used to simulate the flow. The code was developed at the Division of Fluid Dynamics, Department of Applied Mechanics, at Chalmers University of Technology, Göteborg, and is based on the finite volume method. The pressure-velocity coupling is solved using the SIMPLEC algorithm developed by Van Doormaal and Raithby [24]. Conformal block-structured, boundary-fitted coordinates are used, and two ghost cells are employed at the block interfaces to enable different first- and second-order discretization schemes. The code is parallelized by domain decomposition. Message passing interface (MPI) is used for the exchange of information between the different processes/blocks. To avoid spatial oscillations of the pressure field over the collocated (nonstaggered) grid arrangement, Rhie and Chow interpolation is applied for convections through the cell faces. For the discretized and linearized system of equations, TDMA (also known as Thomas' algorithm) and biconjugated gradient solvers are implemented. For this work, a parallelized version of TDMA was used.

4.2 Grids and Numerics. Two different block-structured grids were used in this work. The sizes of the grids were 1,711,424 and 3,356,640 nodes. The two grids will in the following be referred to as the coarse and fine grids, respectively. Each grid consisted of 15 blocks. The block structure is shown in Fig. 2. Each block of the coarse grid consisted of $N_i \times N_j \times N_k = 44 \times 68 \times 44$ nodes except the four wall-bounded blocks of the inlet pipe section, which sum up to $44 \times 68 \times 22$ nodes. The corresponding block sizes of the fine grid are $56 \times 81 \times 51$ and $56 \times 81 \times 31$. For the wall-bounded blocks, N_i, N_j, and N_k refer to the tangential, axial, and radial directions, respectively. The first cell centers normal to the wall were placed at $y^+ \approx 2$ in both grids. Consequently, the coarse grid has larger grid stretching in the wall-normal direction, especially in the inlet pipe section and in the near-wall region just downstream of the sudden expansion. The fine grid has an axial resolution of $\Delta z^+ \approx 50$ and a tangential resolution of $\Delta\theta^+ \approx 20$. The axial and tangential resolutions of the coarse grid are $z^+ \approx 60$ and $\theta^+ \approx 25$, respectively. The approximate values are estimated from a snapshot of the simulation. Both grids are considered fine enough for RANS simulations. The resolution of the fine grid is considered merely adequate for LES. All simulations were made using a second-order central differencing scheme for the momentum and pressure correction equations. The transport equations for k and ω were discretized using the van Leer [25] scheme. The second-order implicit Crank–Nicholson time integration scheme was used. For time-accurate numerical results, a CFL number of CFL < 1 is preferable. With this requirement, nondimensional time steps, $\delta t^* = \delta t \times U_b / D$, of 0.0027 and 0.0036 were sufficient for the fine and coarse grids, respectively, yielding a maximum CFL number of approximately 0.8. Thanks to the larger time step and the smaller grid size, a simulation on the coarse grid is more than twice as fast as a simulation on the fine grid for a specific simulated real-time interval. Time series of the wall pressure at several locations were sampled during the simulations. The

Downloaded 30 Apr 2008 to 129.16.64.122. Redistribution subject to ASME license or copyright; see http://www.asme.org/terms/Terms_Use.cfm

solutions were considered as converged when the pressure levels were fluctuating around a steady mean value (i.e., when the flow was fully developed) and all normalized residuals were of the order of 10^{-3} in each time step. The residuals of the momentum equation were normalized by the global convection and the residuals of the continuity equation were normalized by the mass flow rate. The filtered version of the k-ω model requires slightly more CPU time than the original formulation. Nevertheless, it is expected to be computationally cheaper than most other two-equation models because of the simplicity of the original formulation. The additional cost of computing the function g, Eq. (16), can be compared to that of, e.g., adding a damping function to the eddy viscosity. Furthermore, the convergence rate of the filtered model was much better than the convergence rate of the original model.

4.3 Boundary Conditions and Turbulence Model Constants. Spline curves based on the measured data of Dellenback et al. [14] were used as the inlet boundary condition for the mean velocities. The experimental data taken along two counter-directed radial lines were averaged to obtain a fully symmetric inflow condition. A boundary layer based on the log-law was added between the (radially) outermost measuring point and the wall. Earlier numerical investigations by Schlüter et al. [21] showed that the resolved turbulence level of the inlet boundary conditions has a great effect on the mean velocity profiles for low swirl levels. However, the swirl level in the present study is high enough for a fast transition to turbulence. Hence, to add unsteadiness at the steady inlet boundary condition is superfluous. A constant inlet turbulent intensity of 10% was chosen, and the inlet boundary condition for ω was approximated by $\omega=\sqrt{k}/(\beta^* R)$, where R is the radius of the inlet and a crude estimate of the turbulent length scale. The assumption of a turbulent intensity of 10% was based on the levels of axial and tangential Reynolds normal stresses, as measured by Dellenback et al. [14]. The turbulent intensity of 10% was estimated from measurements by Dellenback et al. The simulations using the filtered k-ω model are not expected to be sensible to the values of turbulent quantities at the inlet boundary. If the imposed length scale is too large, the filter will activate and automatically decrease the production of turbulence via the eddy viscosity, according to Eq. (7). However, this matter has not yet been studied in detail. At the outlet, a homogeneous Neumann boundary condition was used for all variables. A no-slip condition was used for the velocity at the walls, where the turbulent kinetic energy also vanishes. The wall boundary condition for the specific dissipation was set at the first interior node as $\omega=6\nu/(\beta^* y^2)$, see Ref. [20].

Two turbulence models have been considered, i.e., the k-ω model by Wilcox [13] and the wall-adapting local eddy-viscosity (WALE) zero-equation subgrid model by Nicoud and Ducros [26]. The filtering technique derived in Sec. 3.1 was applied only to the former model. A filter width of $\alpha=3$ was chosen for the k-ω model, and $C_w=0.5$ for the WALE model.

5 Results

The purposes of the novel filtering technique are to allow large-scale unsteady structures in the resolved flow field and to give accurate time-averaged results on a typical RANS grid. In order to see what results can be obtained from a LES on the same grid, a simulation using the WALE subgrid turbulence model, derived by Nicoud and Ducros [26], was also made. The WALE model is known to perform very well in complex flows as long as all energy-containing turbulent structures are sufficiently resolved. As will be shown in Sec. 5.2, the grid resolution is, as expected, not fine enough to actually justify the use of the WALE subgrid model. Especially the wall-normal resolution must be higher.

The main features of the flow are visualized and discussed in Sec. 5.1. The time-averaged results of the computations are compared to experiments done by Dellenback et al. [14] in Sec. 5.2.

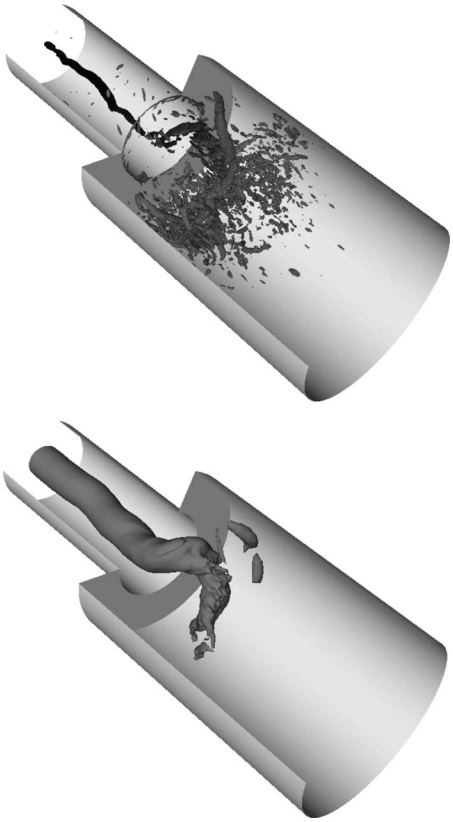

Fig. 3 Snapshot of the precessing vortex core visualized by isosurfaces of the nondimensional second invariant of the velocity gradient, $II^*_{\partial_j U_i}=480$ (top) and static pressure (bottom). Both methods predict the same location and shape of the vortex core. The results are obtained from a simulation using the filtered k-ω model on the fine grid. Only a part of the computational domain is shown. The helicoidal vortex structure is formed immediately after the expansion and propagates upstream almost all the way up to the inlet. It dominates the flow until a point approximately one and a half diameters downstream of where it is formed. At this point, the flow returns to a quasisymmetric mode.

The filter function and the eddy viscosity are examined in Sec. 5.2.2, while the resolved and modeled turbulent kinetic energies are discussed in Sec. 5.2.3. The unsteadiness of the flow is analyzed in Sec. 5.3.

5.1 Visualization of Resolved Structures. A snapshot of the flow is presented in Fig. 3. The vortical structures are visualized by isosurfaces of the nondimensional second invariant of the velocity gradient tensor and pressure. The second invariant of the velocity gradient tensor is normalized by the factor $(R/U_b)^2$ and will in the following be referred to as $II^*_{\partial_j U_i}$. It can be physically interpreted as the source term for the pressure equation, see Ref. [27] for further details. A local maximum of $II^*_{\partial_j U_i}$ is located inside each small volume that is bounded by an isosurface, and corresponds to local pressure minimum. The vortex that is defined at the inlet breaks down near the sudden expansion. A helicoidal vortex core is formed. The vortex core rotates around the geometrical axis of symmetry with a well defined frequency. Other counter-rotating vortex structures are formed in the near-wall recirculation zone just downstream of the expansion. These structures give rise to other frequencies. There is also a recirculation zone along the axis of symmetry, i.e., the flow on the inside of the helicoidal structure is reversed.

A comparison of the results obtained from using different grid

Downloaded 30 Apr 2008 to 129.16.64.122. Redistribution subject to ASME license or copyright; see http://www.asme.org/terms/Terms_Use.cfm

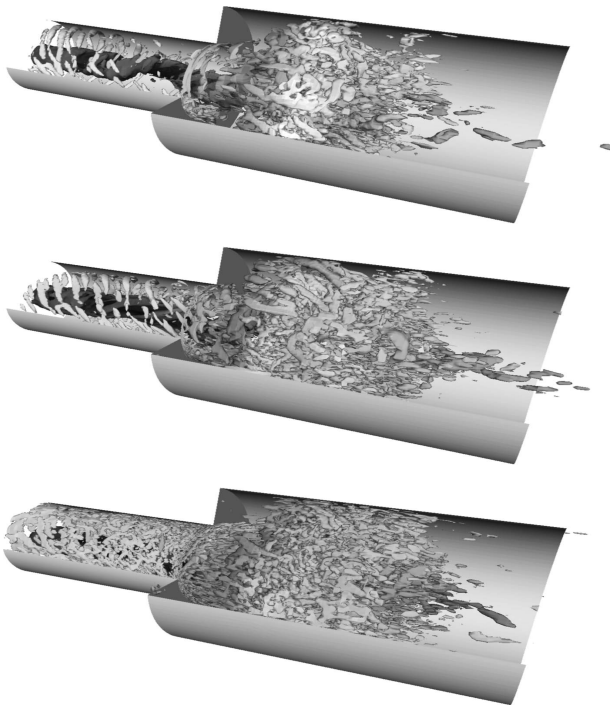

Fig. 4 Isosurfaces of the normalized second invariant of the velocity gradient tensor, $II^*_{\partial_j U_i}=120$, using the filtered k-ω model and the WALE model. Top: filtered k-ω, coarse grid. Center: filtered k-ω, fine grid. Bottom: WALE model, fine grid. The isosurfaces are shaded by the static pressure. A darker shade denotes a lower pressure. As expected, the fine grid resolves a larger part of very small scale turbulence. However, the strongest and largest vortices are well resolved on any of these grids. An even higher density of small-scale turbulence is obtained using the WALE model.

sizes and turbulence models is presented in Fig. 4, where instantaneous isosurfaces of $II^*_{\partial_j U_i}=120$ are shown in Fig. 4. Large torus-shaped vortices are formed near the sudden expansion. The main vortex core is very well defined near the axis of symmetry in the upstream part of the domain. The simulation using the filtered k-ω model on the fine grid resolves a larger part of the small-scale turbulence, as compared with the result of using the same model on the coarse grid, as expected. The WALE model is less dissipative than the filtered k-ω model, resulting in an even higher density of small-scale turbulence.

5.2 Velocity Profiles and Time-Averaged Results. The time-averaged results are based on 1480 samples, which correspond to a nondimensional sampling time of $t^*_S=40$, as there were ten time steps between each sample. This is approximately equivalent to 20 vortex core revolutions or four mean flow residence times. The axisymmetry of the computional domain also allows circumferential averaging, and thus the time-averaged profiles at four circumferential locations were averaged once again. This yields a virtual sampling time of $t^*_S=160$. The evolutions of the axial and tangential velocity distributions and the swirl angle ($\arctan(V_\theta/V_z)$) near the sudden expansion are shown in Fig. 5. The experimental data shown are for each z/D the averages of measurements taken along two counterdirected radial lines.

The agreement between the results obtained from using the filtered k-ω model and the experimental data is excellent. The WALE model also performs quite well. The main differences in the prediction of the axial velocity profiles are found in the most unsteady region, where the vortex breaks down. The swirl velocity far downstream is overestimated by the simulation using the WALE model. On the other hand, the grid resolution may not be at a level that fully justifies the use of this model.

As the length scale of the local grid spacing appears explicitly in the filter function, Eq. (16), it is expected that the instantaneous solution is influenced by a grid refinement. However, the time-averaged solutions should ideally not be sensitive to the grid refinement. Figure 5 suggests that the grid dependence seems not to be a major issue. The results obtained when the filtered k-ω model is used on the coarse grid actually agree better with experimental data than the results obtained from using the WALE model on the fine grid. No study of the performance of the WALE model on the coarse grid has been carried out, simply because it is not applicable. It should be borne in mind that the filtered k-ω simulations on the coarse grid for a specific real-time interval are completed in less than half of the time, as compared to the simulations on the fine grid. The simulations using the WALE model on the fine grid are approximately 30–50% faster than the filtered k-ω approach on the same grid, because fewer equations are being solved.

The original (nonfiltered) k-ω model fails to predict reasonable results. The simulation converges to a steady flow even if an unsteady velocity field obtained from using the filtered k-ω model is used as an initial (starting) condition. Nevertheless, the axial velocity profiles show good agreement with the other simulations near the wall, and the tangential velocity profiles near the suddden expansion, Fig. 5 (second row, to the left), show very good agreement at $r/D>0.5$. The results deteriorate closer to the centerline. Figure 5 (second row, to the right) shows that the rate of decay of swirl is far too high.

It can be shown that the original k-ω model is insensitive to rotation, see, e.g., Ref. [20]. Furthermore, the turbulence model tends to damp out unsteady fluctuations during the simulation. It is clear that the filtering procedure of the turbulent length and time scales removes these inherent shortcomings of the turbulence model, while retaining its good near-wall characteristics.

5.2.1 Reattachment Length. The flow enters the wider pipe section as a swirling jet. The flow separates from the wall at the sudden expansion and a large region of entraining and recirculating flows is formed near the wall of the wider pipe section. The mean axial flow reattaches to the wall at some distance a few (inlet) diameters downstream of the sudden expansion. This distance is called the reattachment length.

Dellenback et al. [14] measured the reattachment length of the flow and obtained a value of $z_r/h=2.5$, where h is the step size, i.e., the difference between the outlet and inlet radii. The average reattachment length obtained from using the filtered k-ω model on the fine grid is $z_r/h=2.5$, in full agreement with the experimental result. A reattachment length of approximately $x_r/h=3.3$ was obtained when using the WALE model. The reattachment length obtained when using the filtered k-ω model on the coarse grid is almost 15% larger compared to the simulation on the fine grid, i.e., $z_r/h\approx 2.9$. The longer reattachment length is directly connected to the slight overshoot of the axial velocity profile at $z/D=1$ and $r/D\approx 0.5$. This can probably be explained in part by the larger grid stretching that was applied in the design of the coarse grid. Nevertheless, as can be seen in Fig. 5, the velocity profiles agree quite well with the experimental data.

5.2.2 Eddy Viscosity and the Filter Function. The time-averaged square of the filter function, Eq. (16), and the filtered eddy viscosity is shown in Fig. 6. The filter function is always inactive near the wall region and sometimes in the strong shear layer near the sudden expansion. In these regions, the modeled turbulent length scales are small enough to pass through the filter. The small turbulent length scales of the shear layer partly originate from the wall boundary layer of the upstream pipe section. The distribution of eddy viscosity is directly influenced by the shape of the filter function. Figure 6 (left) shows that the filter function behaves approximately the same on both grids. The rea-

Downloaded 30 Apr 2008 to 129.16.64.122. Redistribution subject to ASME license or copyright; see http://www.asme.org/terms/Terms_Use.cfm

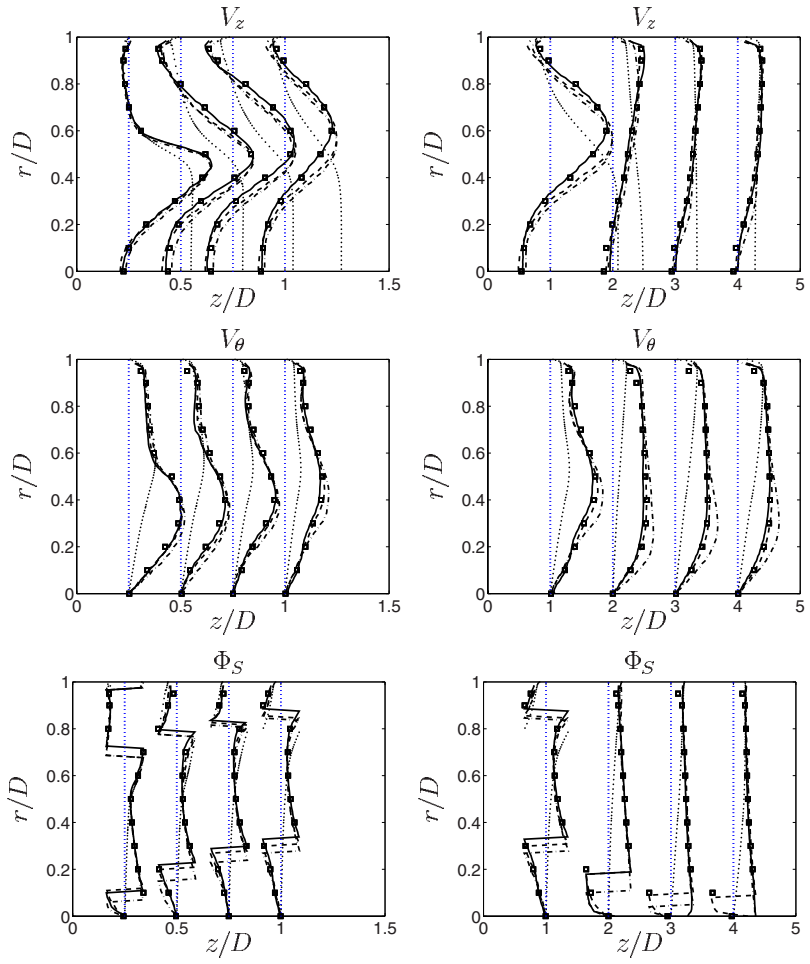

Fig. 5 Radial distributions of averaged axial velocity (top row), tangential velocity (center row), and swirl angle (bottom row) at different cross sections. (—) Filtered *k-ω* model, fine grid. (– – –) Filtered *k-ω* model, coarse grid. (· –) WALE model, fine grid. (···) Standard *k-ω* model, coarse grid. (□) Experiment. The scaling between the left and right columns is given by the profiles at *z/D* =1. The standard *k-ω* model fails to predict reasonable results. It converges to a steady solution. The WALE model performs well considering the grid resolution. However, the agreement between the results obtained using the filtered *k-ω* model and the experimental data is excellent, especially on the fine grid.

sons for this are that less turbulence is modeled on the fine grid and that the denominator of Eq. (16) has decreased in proportion to the nominator, i.e., the filter width. The eddy viscosity, shown in Fig. 6 (to the right), is very dependent on the grid resolution, however. This is actually the advantage of the present approach. When the grid is not fine enough to resolve the turbulent structures, their effect must instead be present through the modeled part of the turbulence. The maximum value of the nondimensional filtered eddy viscosity that is shown in Fig. 6 (to the right) is $\hat{\nu}_t^* = \hat{\nu}_t/\nu = 75$. It is found at $z/D = 0.5$ using the coarse grid. At that location, the fine grid gives a maximum value of $\hat{\nu}_t^* = 59$.

5.2.3 Turbulent Kinetic Energy. Figure 7 shows the distributions of the modeled and the (time-averaged) resolved turbulent kinetic energy (TKE) for the two different grids at two different cross sections, obtained with the filtered k-ω model. The resolved TKE is computed as $K = (\langle \bar{u}_i \bar{u}_i \rangle - U_i U_i)/2$, where $\bar{u}_i$ and U_i are the resolved (instantaneous) and time-averaged velocity vectors, respectively, and $\langle(\cdot)\rangle$ denotes time average. The weak grid dependence of the resolved TKE, K, suggests that it is dominated by large-scale fluctuations. The maximum of resolved turbulent kinetic energy in Fig. 7 (to the left), at $r/D \approx 0.4$, corresponds to the location of the rotating vortex core. Further downstream, at $z/D = 2$, the resolved turbulent kinetic energy is quite evenly distributed.

The grid dependence of the (nonfiltered) modeled TKE, k, is explained by the fact that the filtered eddy viscosity is used in the production term, P_k, in the transport equation for k, i.e., $P_k = 2\hat{\nu}_t S_{ij} \partial_j \bar{u}_i$, where S_{ij} is the strain rate tensor, see, e.g., Ref. [20]. Consequently, the finer the grid, the less turbulence will be modeled.

The distribution of filtered modeled TKE, $\hat{k}$, as defined in Eq. (15), is determined by length and time scales smaller or equal to what can be resolved. It is the only part of the modeled turbulent kinetic energy that is fed to the momentum equations, via the eddy viscosity. From Fig. 7, it is clear that the filtered modeled TKE obtained on the fine grid is approximately one order of magnitude smaller than the resolved TKE, K. In Sec. 5.2.2, it was shown that the filter is inactive in the near-wall region, i.e., $g^2 = 1$ in Eq. (18). Hence, the filtered modeled TKE, $\hat{k}$, is identical to the nonfiltered modeled TKE, k, in the near-wall region. Note that a local maxi-

Downloaded 30 Apr 2008 to 129.16.64.122. Redistribution subject to ASME license or copyright; see http://www.asme.org/terms/Terms_Use.cfm

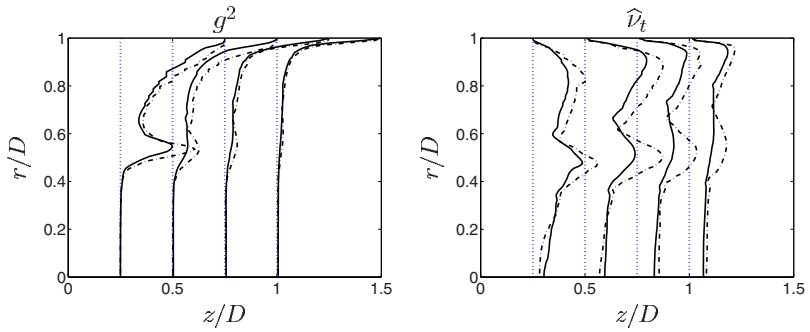

Fig. 6 Radial distribution of the time-averaged squared filter function, g^2 (left), and the (nondimensional) filtered eddy viscosity, $\hat{\nu}_t^* = \hat{\nu}_t/\nu$ (right), obtained with different grids. (· –) Coarse grid. (—) Fine grid. The filter is inactive near the wall where it reaches the value of 1, and (often) in the strong shear layer near the sudden expansion. The filtered eddy viscosity is much larger on the coarse grid, because the less that is resolved, the more must be modeled. The maximum (time-averaged) value of the filtered eddy viscosity, $\hat{\nu}_t^* = 75$, is found at $z/D = 0.5$ (coarse grid).

mum of the filtered modeled TKE occurs at $r/D \approx 0.5$. The maximum coincides with the local maximum of the filter function in Fig. 6 (to the left). It is explained by the fact that nonresolved TKE of the inlet boundary layer is convected downstream into the larger pipe section. This flow-history effect could not have been predicted by anything but a transport model for turbulence.

5.3 Frequency Analysis. The fluctuations of the wall pressure as a function of the nondimensional time are shown in Fig. 8 (to the left). As can be seen, the time series obtained from the two grids are quite similar. The fluctuations are somewhat larger in the simulation on the fine grid. Fourier transforms of the wall pressure were used to analyze the large-scale unsteadiness of the flow. The Fourier transforms of 6609 overlapping segments of length 2^{13} were averaged in order to get rid of the noise. Each segment from the simulation on the fine grid, in which a nondimensional time step of 0.0027 was used, corresponds to a nondimensional sampling time $t^* \approx 22$. Figure 8 (to the right) shows that the resolution seems not to play a major role in determining the main frequency. The most distinct nondimensional frequency is at Strouhal number $\mathrm{St} = f \times U_b/D = 0.6$. This frequency corresponds to the rotational speed of the helicoidal vortex core.

Figure 9 shows the spectral density of the wall pressure sampled at four different downstream locations. Near the expansion, the solution obtained using the filtered k-ω model shows exactly the same frequency as the solution obtained by using the WALE model. This is expected, as the vortex core is fully resolved in both simulations. The lower frequencies most likely correspond to the bursting of large turbulent structures in the recirculation zone near the wall, just after the expansion, as these structures are convected downstream. As the vortex core does not propagate further downstream than to where the flow reattaches, only the lower frequencies are present downstream $z/D \approx 1.25$. Because of the limited sampling time, the lowest frequencies are not well resolved. Hence, the model and grid dependency of the lowest frequencies cannot be analyzed.

Figure 10 shows the normalized frequency spectra of resolved

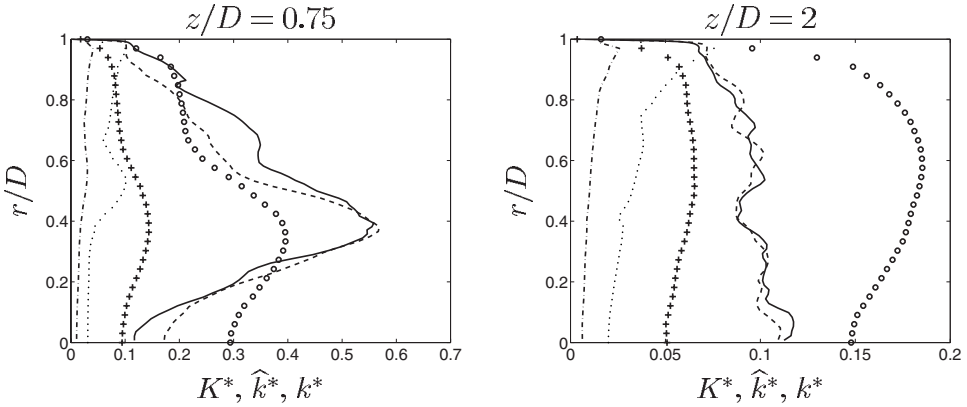

Fig. 7 Radial distribution of nondimensional turbulent kinetic energy (TKE) at $z/D = 0.75$ (left) and $z/D = 2$ (right) obtained with the filtered k-ω model on two different grids. All quantities marked by superscript asterisks (*) are normalized by U_b^2. (– –) Resolved TKE (K^*), coarse grid. (—) Resolved TKE (K^*), fine grid. (···) Filtered modeled TKE ($\hat{k}^*$), coarse grid. (-·) Filtered modeled TKE ($\hat{k}^*$), fine grid. (○) Modeled TKE (k^*), coarse grid, (+) Modeled TKE (k^*), fine grid. The resolved TKE is dominated by large-scale turbulent structures that only weakly depend on grid resolution. The distribution of filtered modeled turbulent kinetic, $\hat{k}^*$, is determined by length and time scales smaller or equal to what can be resolved. Consequently, it depends heavily on grid resolution.

Downloaded 30 Apr 2008 to 129.16.64.122. Redistribution subject to ASME license or copyright; see http://www.asme.org/terms/Terms_Use.cfm

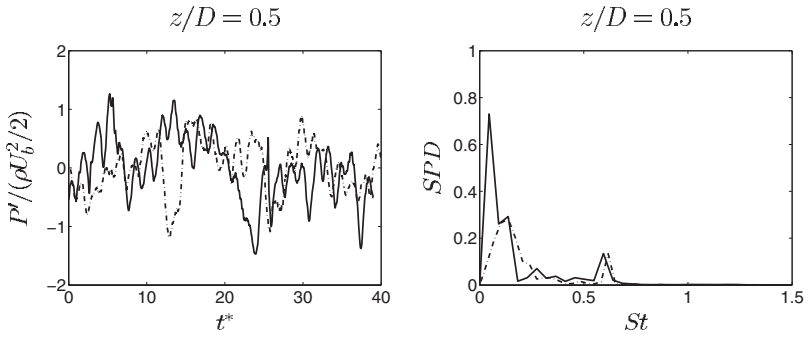

Fig. 8 Left: time series of nondimensional wall pressure fluctuations at $z/D = 0.5$ obtained with the filtered k-ω model. (—) Fine grid. (– –) Coarse grid. Note that the end points of the time series are quite arbitrary, and thus no correlation between the two series is expected. Right: spectral power density of the wall pressure at $z/D = 0.5$ obtained from using the filtered k-ω model. (—) Fine grid. (– –) Coarse grid. The predicted rotational speed (St=0.6) of the vortex core is not sensitive to the resolution.

axial velocity fluctuations at $z/D=2$ and $r/D=0.25$, obtained using the filtered k-ω model on different grids. The largest scales of turbulence are resolved on both grids, as already seen in Fig. 7. However, there is a difference in the prediction of intermediate- and small-scale turbulences. At the locations $z/D=2$ and $r/D=0.25$, the grids are not fine enough to resolve turbulent structures with frequencies higher than St$\sim$20. The results for higher frequencies are accordingly not included in Fig. 10.

6 Conclusions

Numerical simulations of unsteady turbulent flow can be significantly improved by applying an adaptive low-pass filter to the modeled turbulent length and time scales predicted by a two-equation low Reynold number (LRN) turbulence model. The filter limits the damping effect of the turbulent viscosity on the resolved flow field away from walls. Large-scale unsteady turbulent structures are resolved, and the time-averaged results correspond very well to experimental data. On the computational grids considered in this work, the filtered k-ω model surpasses the WALE LES model in accuracy, while the results are equivalently unsteady. The main frequency of the simulated flow is not sensitive to the choice of model or grid size, while the amplitude of the largest pressure fluctuations is. The difference in the prediction of the largest scales is most likely connected to the difference in the prediction of the reattachment length. While the simulation using the filtered k-ω model agrees very well with experimental results

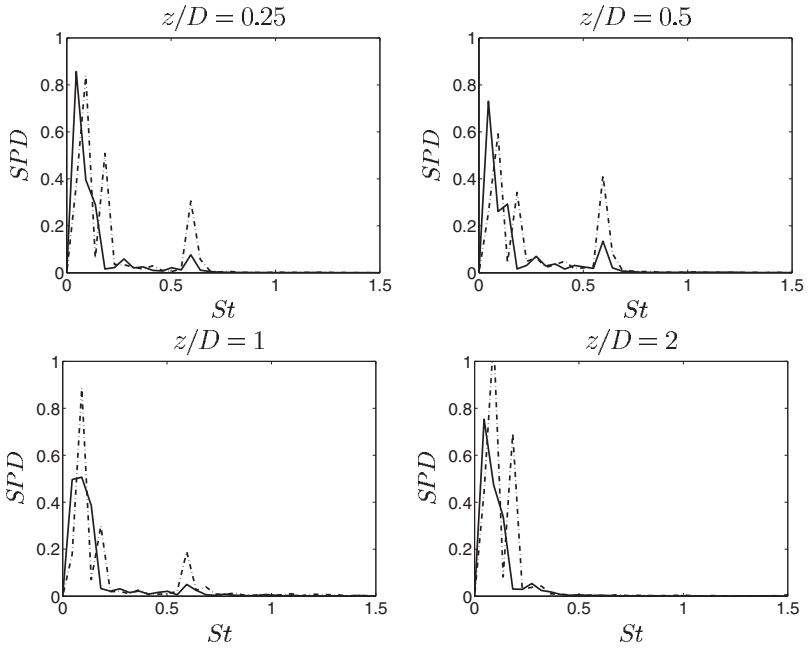

Fig. 9 Spectral power density of the wall pressure fluctuations at $z/D=0.25$ (top left), $z/D=0.5$ (top right), $z/D=1$ (bottom left), and $z/D=2$ (bottom right). (—) Filtered k-ω model, fine grid. (· –) WALE model, fine grid. The most distinct frequency is at St=0.6 and corresponds to the rotational speed of the vortex core. The strong lower frequencies most likely correspond to unsteady structures that are formed in the recirculation zone near the wall, just after the expansion.

Downloaded 30 Apr 2008 to 129.16.64.122. Redistribution subject to ASME license or copyright; see http://www.asme.org/terms/Terms_Use.cfm

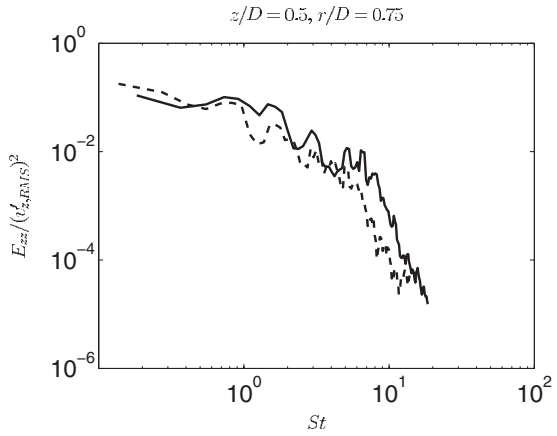

Fig. 10 Normalized frequency spectra of resolved axial velocity fluctuations at $z/D=2$ and $r/D=0.75$ using the filtered k-ω model on two grids. (—) Fine grid. (– –) Coarse grid. (· –) Note the higher density of high frequencies obtained when using the fine grid.

in this respect as well, the estimate of the reattachment length obtained from the simulation using the WALE model is not satisfactory.

It was shown by Gyllenram and Nilsson [18] that the degree of unsteadiness in the resolved velocity field is inversely related to the size of the filter width, i.e., model coefficient α. However, too small a filter width may cause the results to deteriorate because there will be a spectral gap between the filtered scales and the scales that can potentially be resolved. Furthermore, it is preferable for the filter width to be large enough to enable the original asymptotic near-wall behavior of the turbulence model. The positive effects of introducing the filtering technique to the present test case most likely owe to a more accurate prediction of the large-scale unsteadiness. As shown by Gyllenram et al. [22], the turbulence is, at least in a time-averaged sense, extremely anisotropic in the shear layer near the sudden expansion. However, most of the anisotropy lies in the largest scales. If the large anisotropic scales are accurately resolved in space and time, a simple turbulence model is sufficient for estimating the influence of small-scale turbulence on the mean flow.

A study of the influence of the grid resolution was carried out. The local grid resolution is explicitely used in the formulation of the eddy viscosity when the filter is active. This will obviously introduce a grid dependence in the instantaneous flow field, and the time-averaged results are also expected to be affected. In spite of this, the grid dependence of the time-averaged results seems surprisingly weak and may just as well be a numerical issue. Neither were the main unsteady effects sensitive to the spatial resolution.

Acknowledgment

This project was financed by SVC:[1] Swedish Energy Agency, ELFORSK, Svenska Kraftnät. The authors would also like to thank Dr. Ruprecht at IHS, University of Stuttgart, for support during the development of the model, and Dr. Paul A. Dellenback at the University of Wyoming, USA, for providiing the experimental data.

[1]Companies involved: CarlBro, E.ON Vattenkraft Sverige, Fortum Generation, GE Energy (Sweden), Jämtkraft, Jönköping Energi, Mälarenergi, Skellefteå Kraft, Sollefteåforsens, Statoil Lubricants, Sweco VBB, Sweco Energuide, SweMin, Tekniska Verken i Linköping, Vattenfall Research and Development, Vattenfall Vattenkraft, Waplans, and VG Power and Öresundskraft. Universities involved: Chalmers University of Technology, Luleå University of Technology, Royal institute of Technology, and Uppsala University.

References

[1] Spalart, P. R., 2000, "Strategies for Turbulence Modeling and Simulations," Int. J. Heat Fluid Flow, **21**, pp. 252–263.
[2] John, V., 2006, "Short Review of Some Aspects in LES and VMS," Appl. Math. (Germany), **51**, pp. 321–353.
[3] Speziale, C. G., 1998, "Turbulence Modeling for Time-Dependent RANS and VLES: A Review," AIAA J., **36**, pp. 173–184.
[4] Speziale, C. G., 1998, "A Combined Large-Eddy Simulation and Time-Dependent RANS Capability for High-Speed Compressible Flows," J. Sci. Comput., **13**(3), pp. 253–274.
[5] Fasel, H. F., Seidel, J., and Wernz, S., 2002, "A Methodology for Simulations of Complex Turbulent Flows," J. Fluids Eng., **124**, pp. 933–942.
[6] Spalart, P. R., Jou, W.-H., Strelets, M., and Allmaras, S. R., 1997, "Comments on the Feasibility of LES for Wings, and on a Hybrid RANS/LES Approach," *Advances in DNS/LES, First AFOSR International Conference on DNS/LES*, Ruston, LA, Aug. 4–8, C. Liu and Z. Liu, eds. Greyden, Columbus, OH.
[7] Menter, F., Kuntz, M., and Egerov, Y., 2003, "A Scale Adaptive Simulation Model for Turbulent Flow Predictions," 41st AIAA Aerospace Sciences Meeting and Exhibit, Reno, NV, Vol. AIAA-2003-0767.
[8] Menter, F. R., Kuntz, M., and Langtry, R., 2003, "Ten Years of Industrial Experience With the SST Turbulence Model," in *Turbulence, Heat and Mass Transfer*, Begell House, New York, Vol. 4.
[9] Kok, J. C., Dol, H. S., Oskam, B., and van der Ven, H., 2004, "Extra-Large Eddy Simulation of Massively Separated Flows," 42nd AIAA Aerospace Meeting, Reno, NV, pp. 1–12.
[10] Menter, F. and Egerov, Y., 2005, "A Scale Adaptive Simulation Model Using Two-Equation Models," 45th AIAA Aerospace Sciences Meeting and Exhibit, Reno, NV, Vol. AIAA-2005–1095.
[11] Templeton, J. A., Medic, G., and Kalitzin, G., 2005, "An Eddy-Viscosity Based Near-Wall Treatment for Coarse Grid Large-Eddy Simulation," Phys. Fluids, **17**, p. 105101.
[12] Willems, W., 1996, "Numerische Simulation Turbulenter Scherströmungen mit einem Zwei-Skalen Turbulenzmodell," Ph.D. thesis, Rheinish-Westfälischen Technischen Hochschule, Aachen, Germany.
[13] Wilcox, D. C., 1988, "Reassessment of the Scale-Determining Equation for Advanced Turbulence Models," AIAA J., **26**(11), pp. 1299–1310.
[14] Dellenback, P. A., Metzger, D. E., and Neitzel, G. P., 1987, "Measurements in Turbulent Swirling Flow Through an Abrupt Expansion," AIAA J., **26**(6), pp. 669–681.
[15] Durbin, P. A., 1995, "On the k-ε, Stagnation Point Anomaly," Int. J. Heat Fluid Flow, **17**, pp. 88–89.
[16] Helmrich, T., Buntic, I., and Ruprecht, A., 2002, "Very Large Eddy Simulation for Flow in Hydraulic Turbo Machinery," *Classics and Fashion in Fluid Mechanics*, Belgrade, Yugoslavia, October 18–20.
[17] Ruprecht, A., Helmrich, T., and Buntic, I., 2003, "Very Large Eddy Simulation for the Prediction of Unsteady Vortex Motion," *Conference on Modeling Fluid Flow, CMFF'03*, 12th International Conference on Fluid Flow Technologies, Budapest, Hungary, September 3–6.
[18] Gyllenram, W. and Nilsson, H., 2006, "Very Large Eddy Simulations of Draft Tube Flow," 23rd IAHR Symposium, Yokohama, Japan, Oct., Vol. 1.2, pp. 1–10.
[19] Batten, P., Goldberg, U., and Chakravarthy, S., 2002, "LNS—An Approach Towards Embedded LES," 40th AIAA Aerospace Sciences Meeting and Exhibit, Reno, NV, Vol. AIAA-2002-0427.
[20] Wilcox, D. C., 2002, *Turbulence Modeling for CFD*, 2nd ed., DCW Industries Inc., La Cañada, CA.
[21] Schlüter, J. U., Pitsch, H., and Moin, P., 2004, "Large Eddy Simulation Inflow Conditions for Coupling With Reynolds-Averaged Flow Solvers," AIAA J., **42**(3), pp. 478–484.
[22] Gyllenram, W., Nilsson, H., and Davidson, L., 2006, "Large Eddy Simulation of Turbulent Swirling Flow Through a Sudden Expansion," 23rd IAHR Symposium, Yokohama, Japan, Oct., Vol. 1.2, pp. 1–10.
[23] Nilsson, H., 2002, "Numerical Investigations of Turbulent Flow in Water Turbines," Ph.D. thesis, Chalmers University of Technology, Göteborg, Sweden.
[24] Van Doormaal, J. P. and Raithby, G. D., 1984, "Enhancements of the SIMPLE Method for Predicting Incompressible Fluid Flows," Numer. Heat Transfer, **7**, pp. 147–163.
[25] van Leer, B., 1974, "Towards the Ultimate Conservative Difference Scheme Monotonicity and Conservation Combined in a Second Order Scheme," J. Comput. Phys., **14**, pp. 361–370.
[26] Nicoud, F. and Ducros, F., 1999, "Subgrid-Scale Stress Modelling Based in the Square of the Velocity Gradient Tensor," Flow, Turbul. Combust., **62**, 183–200.
[27] Jeong, J., and Hussain, F., 1995, "On the Identification of a Vortex," J. Fluid Mech., **285**, pp. 69–94.

Downloaded 30 Apr 2008 to 129.16.64.122. Redistribution subject to ASME license or copyright; see http://www.asme.org/terms/Terms_Use.cfm